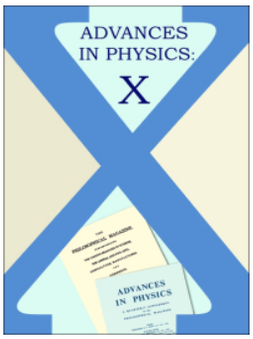

Advances in Physics: X

ISSN: (Print) (Online) Journal homepage: www.tandfonline.com/journals/tapx20

Simulating micromagnetism

Razyeh Behbahani Diba, Martin L. Plumer & Ivan Saika-Voivod

To cite this article: Razyeh Behbahani Diba, Martin L. Plumer & Ivan Saika-Voivod (2024) Simulating micromagnetism, Advances in Physics: X, 9:1, 2409070, DOI: 10.1080/23746149.2024.2409070

To link to this article: https://doi.org/10.1080/23746149.2024.2409070

Published online: 21 Oct 2024.

ADVANCES IN PHYSICS: X
2024, VOL. 9, NO. 01, 1–30
https://doi.org/10.1080/23746149.2024.2409070

Taylor & Francis
Taylor & Francis Group

REVIEWS

Simulating micromagnetism

Razyeh Behbahani Diba[a,b], Martin L. Plumer[b] and Ivan Saika-Voivod[b]

[a]Department of Physics and Astronomy, University of Western Ontario, London, ON, Canada and [b]Department of Physics and Physical Oceanography, Memorial University of Newfoundland, St. John's, NL, Canada

ABSTRACT

We present an introductory review of concepts behind micromagnetic simulations, in which magnetic moments representing collections of atomic spins within a material evolve according to the Landau-Lifshitz-Gilbert equation, a generalized torque equation. This evolution is determined by a variety of interactions, including those arising from external fields, magnetostatic and exchange effects, and magnetic anisotropy. Anisotropy is a key ingredient in the Stoner-Wohlfarth model, which provides a quantitative basis for understanding magnetic hysteresis. In turn, hysteresis loops provide a basis for comparing simulations and experiments, and are important, for example, in quantifying the heating response of a sample to an oscillating external magnetic field. Micromagnetic simulations bear conceptual similarity to molecular dynamics (MD) simulations, but whereas in MD classical potentials are used to naturally model interactions between atoms and/or molecules, the choice of modelling length scale in micromagnetics is less obvious. If effective interactions are determined for, say, two crystallographic unit cells of a material, how interaction parameters should scale with micromagnetic simulation cell size, particularly at finite temperature, is still an area of research. Finally, we discuss the coupling of magnetic and mechanical degrees of freedom in simulating atomic and nanoparticle systems. This review is based, in part, on our own experience in modelling hysteretic heating of magnetite nanoparticles.

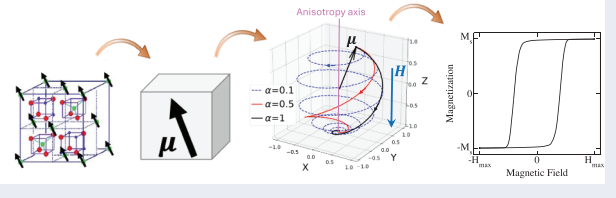

ARTICLE HISTORY
Received 7 June 2024
Accepted 22 September 2024

KEYWORDS
Micromagnetic simulations; Landau-Lifshitz-Gilbert equation; magnetic hysteresis; magnetic nanoparticles

CONTACT Ivan Saika-Voivod saika@mun.ca Department of Physics and Physical Oceanography, Memorial University of Newfoundland, St. John's, NL A1B 3X7, Canada

1. Introduction

Magnetism is a phenomenon that exerts its influence in different contexts on vastly different length scales [1], from the magnetohydrodynamics of galactic collisions [2], to the control of tiny electric currents based on the spins of individual electrons in so-called spintronics [3]. Micromagnetism is devoted to the study of magnetic phenomena with spatial dimensions between the macroscopic and the atomic [4], between solving Maxwell's equations in order to, say, determine the magnetic field configuration due to a tangle of electrical currents, and calculating the quantum mechanical response of atomic nuclei to variations of such a field [5]. In micromagnetic modelling, or simply micromagnetics [6–8], a single classical magnetization vector is used to represent all the atomic spins within a small volume, referred to as a micromagnetic cell, thus treating materials as being composed of a discrete collection of small magnets. The focus of micromagnetic modelling is on physical phenomena occurring on length scales larger than the cell size. The micromagnetic cell is a modelling element that is coarser than, but nonetheless analogous to, an atom or molecule in a molecular dynamics simulation: large enough to be modelled classically, and small enough so that their collective behaviour predicts emergent properties. Examples of applications of micromagnetic modelling include the study and development of magnetic recording media and devices [9–11], thin films [12–15], spintronics [16–18], nanoparticle hyperthermia [19–23] and skyrmions [24–26].

Figure 1 provides an example illustrating the basic idea behind micromagnetic modelling and is motivated by our own efforts in modelling the heating of complex iron oxide nanoparticles under an external AC magnetic field in the context of nanoparticle hyperthermia [27–30]. A small portion of a magnetite nanorod, initially taken to be the crystallographic unit cell comprising several atomic spins highly correlated through strong exchange interactions, is modelled with a coarse-grained micromagetic cell with volume V, uniform magnetization $\mathbf{M}$, and magnetic moment $\boldsymbol{\mu} = \mathbf{M}V$ of constant magnitude $\mu = M_s V$, where M_s is the saturation magnetization [31–33], the magnitude of the magnetic moment per unit volume when

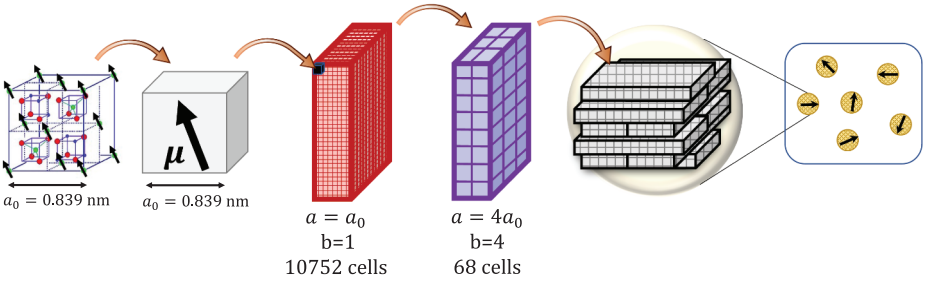

Figure 1. Micromagnetics in a nutshell.

atomic spins are optimally aligned with an external field. This micromagnetic cell interacts with neighbouring cells via exchange and with the many other cells making up the nanorod through magnetostatic (approximately dipolar) interactions. Using larger and therefore fewer micromagnetic cells would reduce the computational load, enabling, in our example, the simulation of assemblies of nanorods in the form of nanoparticles. However, the assumption that all atomic spins are completely correlated owing to exchange within a cell, even at temperature $T = 0$, holds at best only for cells smaller than the *exchange length*, a length scale brought about by the competition between magnetostatic and exchange interactions [4]. At finite T, thermal fluctuations necessitate the finding of effective interaction parameters as a function of V. Beyond the purely magnetic behaviour of a system, there is growing interest in modelling the coupling of magnetic and rototranslational degrees of freedom at the atomistic and nanoscopic scales, for example in the modelling of cobalt nanowires [34] or how nanoparticle rotation can effect hysteretic heating induced by an oscillating external field [35].

The purpose of this review is to familiarize the non-expert reader with the basics of micromagnetic modelling. In section 2, we discuss the interactions and modelling needed to describe magnetic hysteresis, including magnetic anisotropy and the celebrated Stoner-Wohlfarth model. Section 3 provides a discussion of other important magnetic interactions. The equation at the heart of modelling the dynamics of micromagnetics, namely the Landau-Lifshitz-Gilbert (LLG) equation, is presented in section 4. At its core, micromagnetics is an exercise in coarse-graining – using a relatively small number of degrees of freedom with effective interactions between them to represent systems with a large number of individual magnetic spins. In this vein, section 5 discusses how the interactions between micromagnetic cells need to change as cell size is varied. In section 6, we provide a survey of efforts to combine magnetic and mechanical degrees of freedom, a topic gaining recent attention within the micromagnetics community, both on an atomic scale and at the nanoparticle level. In section 7, we provide concluding remarks.

2. Energy, anisotropy and the Stoner-Wohlfarth model: hysteresis

2.1. Energy of a magnetic moment in a field

The fundamental starting point for our discussion is a result familiar to us from the early years of our physics education, namely, that the potential energy (Zeeman energy) of a magnetic dipole, or in our case a uniformly magnetized cell, in a magnetic field $\mathbf{B}$ (or $\mathbf{H}$) is given by,

$$U = -\boldsymbol{\mu} \cdot \mathbf{B} = -\mu_0 \boldsymbol{\mu} \cdot \mathbf{H} = -\mu_0 V \mathbf{M} \cdot \mathbf{H} = -\mu_0 M_s V \mathbf{m} \cdot \mathbf{H}, \qquad (1)$$

where the unit vector $\mathbf{m} = \boldsymbol{\mu}/\mu = \mathbf{M}/M_s$ and $\mu_0 = 4\pi \times 10^{-7}$ N/A^2 is the permeability of free space. In the micromagnetic context of moments within a magnetic material, $\mathbf{H}$ is not solely due to an external field. Magnetocrystalline anisotropy, arising from the electronic environment formed by the neighbours of magnetic ions, various forms of exchange, and weak but long-ranged magnetostatic (dipolar) fields are possible contributors to the effective field acting on a given magnetic moment. Going forward, we will refer to the external field as $\mathbf{H}$, and the effective field as $\mathbf{H}_{\text{eff}}$. Whatever the sources of $\mathbf{H}_{\text{eff}}$, $\boldsymbol{\mu}$ will align with it if energy is removed from the system.

2.2. Magnetic anisotropy

While less familiar to students of physics than exchange and dipolar interactions, magnetic anisotropy is important in understanding magnetic hysteresis loops, which are crucial in characterizing magnetic materials and systems experimentally [31,32,36–38].

Crystal structure, shape and surfaces of a magnetic sample can result in magnetic anisotropy: preferred directions for the magnetic moments within the sample. *Magnetocrystalline anisotropy* arises from the *crystal field*, defined as the electric field arising from neighbouring atoms in the crystal [32]. It derives its character from the symmetry of the local environment. For a uniaxial crystal, this energy depends on the angle the spin makes with the anisotropy axis represented by the unit vector $\mathbf{u}$, and its contribution to the system Hamiltonian can be written as,

$$\mathcal{H}_{\text{ani}} = -K_u V(\mathbf{m} \cdot \mathbf{u})^2, \tag{2}$$

where K_u is the uniaxial magnetocrystalline anisotropy constant or energy density. When $K_u > 0$ ($\mathbf{u}$ defines an *easy axis*), the energy is lower if the moment aligns, either parallel or antiparallel, with $\mathbf{u}$, and if $K_u < 0$ ($\mathbf{u}$ defines a *hard axis*), the energy is minimized when spins lie in a plane perpendicular to $\mathbf{u}$. For a cubic crystal with three equally preferred axes, taken here as $\hat{\mathbf{x}}$, $\hat{\mathbf{y}}$, $\hat{\mathbf{z}}$, the lowest order anisotropy term occurs at fourth order, given by, $\mathcal{H}_{\text{ani}} = -K_c V(m_x^4 + m_y^4 + m_z^4)$, where K_c represents the cubic anisotropy constant. $K_c > 0$ causes spins to align along the [100] directions and for $K_c < 0$ the preferred anisotropy axes are along [111].

Surface anisotropy originates from broken symmetry at the surface and surface-core strains. It imparts a local anisotropy axis perpendicular to the surface and can be orders of magnitude greater than bulk magnetocrystalline anisotropy, for example, in cubic ferromagnets [39]. The shape of a magnetized object may give rise to *shape anisotropy*, which we discuss below.

2.3. The Stoner-Wohlfarth model and hysteresis loops

The elements discussed above allow us to introduce the Stoner-Wohlfarth (SW) model, the foundational model for understanding hysteresis loops that consists of a uniformly magnetized body with a single uniaxial anisotropy axis, or, more fully, a collection of such independent bodies randomly oriented, subject to an external field. Relevant vectors of the model are illustrated in Figure 2(a). A particle's energy is the sum of the anisotropy and Zeeman contributions, and so it is convenient to work in terms of the reduced external field $h = H/H_k$, where H is the scalar in $\mathbf{H} = H\hat{\mathbf{H}}$, and $H_k = 2K_u/(\mu_0 M_s)$ is called the anisotropy field. Normally, $\hat{\mathbf{H}}$ is considered fixed (often taken to be $\hat{\mathbf{z}}$), with $\mathbf{H}$ flipping directions when H changes sign. A particle's energy depends on the angle θ between the magnetization and the anisotropy (between $\mathbf{m}$ and $\mathbf{u}$), the angle θ_0 between the applied field and the anisotropy axis (between $\hat{\mathbf{H}}$ and $\mathbf{u}$), and the angle between the magnetization and the applied field, which for planar geometry is $\theta_0 - \theta$, and can be expressed in this case as,

$$\frac{E}{K_u V} = \sin^2\theta - 2h\cos(\theta_0 - \theta). \tag{3}$$

As shown in Figure 2(b), for which $\hat{\mathbf{H}}$ is pointing away from $\mathbf{u}$ at an angle of $\theta_0 = 3\pi/4$, energy minima representing the stable and metastable directions of $\boldsymbol{\mu}$ are separated by an energy barrier at low h. Varying h alters these directions. In the low-temperature limit ($T = 0$), on increasing h, $\boldsymbol{\mu}$ initially aligned along $\mathbf{u}$ flips to align (approximately) along $\mathbf{H}$ only when the energy maximum and metastable minimum disappear by merging into an inflection

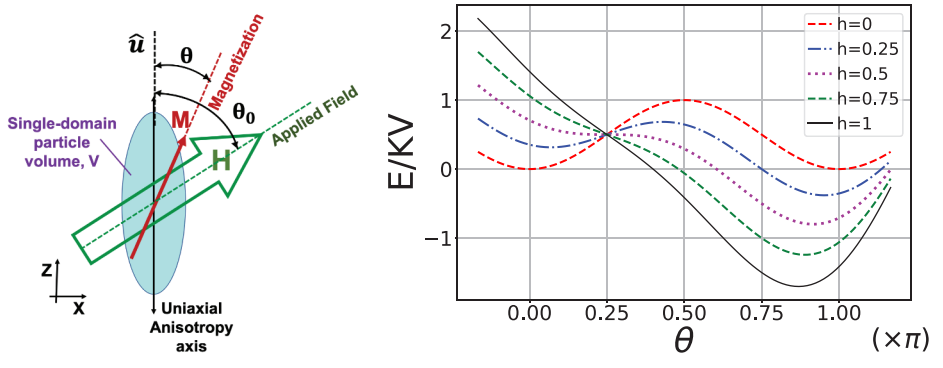

Figure 2. a) Stoner-Wohlfarth particle with an effective uniaxial anisotropy under application of an external field, b) the reduced energy ($E_{\text{tot}}/K_u V$) as a function of θ, when $\theta_0 = 3\pi/4$ and $h_c \simeq 0.5$ (see Equation 3). For $h < 0.5$, two energy minima are present, and they are separated by a maximum. At a threshold value of $h \approx 0.5$ the metastable minimum merges with the maximum, and so for $h \geq 0.5$, there is only a single energy minimum.

point at $h = h_c$ [$h_c \approx 0.5$ in Figure 2(b)], an expression for which is obtainable by considering appropriate derivatives of Equation 3 [31]. For $T > 0$, the required energy to overcome the barrier can be supplied through thermal fluctuations in a statistical process.

Equation 3 forms the basis for understanding hysteresis loops at $T = 0$. Highlighted in Figure 3(a) is a blue hysteresis loop for $\theta_0 = 45°$. At large positive h, $\mathbf{m}$ is nearly aligned with the external field and its component along the field $m_H = \mathbf{m} \cdot \hat{\mathbf{H}}$ is nearly unity. As h decreases and the relative influence of anisotropy increases, m_H decreases, its precise value obtainable by minimizing Equation 3 with respect to θ. At $h = 0$, by definition, $m_H = m_r$, the remanent magnetization. As h decreases further to small negative values, the magnetization is now trapped in a local energy minimum, with the global minimum existing at larger value of θ, as depicted in the inset to the right of Figure 3(a). At $h = -h_c$ the metastable minimum becomes unstable, as depicted in the inset to the top left of Figure 3(a). Infinitesimally below $-h_c$, the magnetization flips to (nearly) align itself again with the external field. In general, the field magnitude H_c at which $m_H = 0$ is called the coercivity, or coercive field. Below $-h_c$, m_H approaches -1 as h decreases further. On increasing h, there is a similar lag in the response of m to the changing sign of h, resulting in an open loop, with a finite area between increasing and decreasing field branches. Loops for other values of θ_0 are shown in Figure 3(a), while the uniformly spherical average over θ_0 is shown in Figure 3(b). This average represents the response of a collection of randomly oriented SW particles.

At finite temperature, thermal excitations facilitate the magnetization switching between energy minima, reducing both m_r and H_c. The rate of switching is chiefly controlled by the energy barrier separating the two minima. Usov et al. [40] introduced expressions for the rate of escape from a local minimum to the global minimum that can be used to calculate hysteresis loops at finite T.

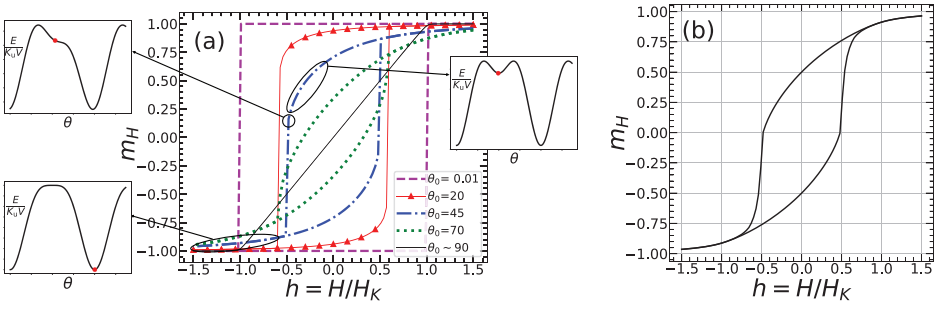

Figure 3. SW hysteresis at $T = 0$: a) hysteresis loop for selected θ_0 and magnetization energy profile according to the field strength; b) average hysteresis loop for a collection of randomly oriented particles.

Hysteresis loops in general depend on both T and the rate at which H changes with time, the sweep rate, which is expressed in terms of the field amplitude and the frequency [41]. The idealized $T = 0$ hysteresis loops reflect the assumption that the sweep rate is effectively zero, i.e. slow enough to allow $\mathbf{m}$ to relax to the local potential energy minimum at every value of H. Simulating this case involves numerical minimization of the energy to a specified tolerance to obtain $m_H(H)$. This approach is sufficient for some applications. In other applications, such as nanoparticle hyperthermia, the sweep rate can strongly impact loops because it is comparable to the relaxation rate of $\mathbf{m}$. The experimental sweep rate can often be orders of magnitude too slow to be accessible to direct simulations. One approach to bridge this gap, in the case when the underlying relaxation follows Arrhenius dynamics, is to link the behaviour of loops at slow sweep rates and low T with those at higher sweep rates and higher T [10]. Additionally, kinetic Monte Carlo techniques are useful when relaxation is dominated by rare energy barrier crossings. In this case, a simulation proceeds at the level of spin flips between stochastic wait times, rather than waiting for flips to occur spontaneously as spins undergo microscopic motion. Kinetic Monte Carlo, however, requires a determination of the escape rates from local energy minima from an analysis of the potential energy landscape [41]. As a final remark, for the case of a finite sweep rate, loop shape falls roughly into two categories: major loops, for which m_H reaches saturation at large H, and minor loops, for which m_H does not plateau at large H but rather traces out an ellipse-like shape in the m_H-H plane.

3. Exchange, dipolar interactions, magnetostatics

3.1. Exchange interactions

The exchange interaction between atoms is a quantum mechanical effect due to the requirement that the wave function for a system of electrons be antisymmetric with respect to the exchange of electrons [32,42,43]. For a system of two electrons, with $\psi_a(\mathbf{r}_1)$ describing the spatial state of the first electron and $\psi_b(\mathbf{r}_2)$ that of the second, the allowed states are the *singlet* and *triplet* states, given respectively by,

$$\begin{aligned}\Psi_{\mathrm{S}} &= \frac{1}{\sqrt{2}}[\psi_a(\mathbf{r}_1)\psi_b(\mathbf{r}_2) + \psi_a(\mathbf{r}_2)\psi_b(\mathbf{r}_1)]\chi^{\mathrm{Singlet}} \text{ and} \\ \Psi_{\mathrm{T}} &= \frac{1}{\sqrt{2}}[\psi_a(\mathbf{r}_1)\psi_b(\mathbf{r}_2) - \psi_a(\mathbf{r}_2)\psi_b(\mathbf{r}_1)]\chi^{\mathrm{Triplet}},\end{aligned} \tag{4}$$

where χ^{Singlet} is a spin state antisymmetric with respect to electron exchange and with total spin $S = 0$, and χ^{Triplet} represents any of three symmetric states with total spin $S = 1$. The spatial parts are constructed to be appropriately symmetric or antisymmetric.

The energy difference between singlet and triplet states can be written in terms of an overlap integral,

$$E_{\mathrm{S}} - E_{\mathrm{T}} = 2J = 2 \int \psi_a^*(\mathbf{r}_1)\psi_b^*(\mathbf{r}_2)\mathcal{H}\psi_a(\mathbf{r}_2)\psi_b(\mathbf{r}_1)d\mathbf{r}_1 d\mathbf{r}_2, \tag{5}$$

which depends on Coulomb interactions and is zero if ψ_a and ψ_b do not overlap.

The widely used Heisenberg model Hamiltonian can then be written, up to a constant, as,

$$\mathcal{H}_H = -2J\mathbf{S}_1 \cdot \mathbf{S}_2, \tag{6}$$

where the eigenvalues of the operator $\mathbf{S}_1 \cdot \mathbf{S}_2$ are $-\frac{3}{4}$ for χ^{Singlet} and $\frac{1}{4}$ for χ^{Triplet}. For $J < 0$, the singlet state, for which spins are antialigned, has the lower energy, giving rise to antiferromagnetic order. Conversely, for $J > 0$, the triplet state has lower energy, giving rise to ferromagnetic order. While the quantum states of a system with many spins is much more complex, pairwise exchange is still relevant. In the classical version of the Heisenberg model, the spin operators are replaced with classical spin vectors.

In making the transition to micromagnetics, the exchange energy of the system takes on the form of the classical Heisenberg model,

$$E = -\sum_{<i,j>} J_{\mathrm{eff}}\mathbf{m}_i \cdot \mathbf{m}_j, \tag{7}$$

where the double sum runs over all nearest neighbour pairs of cells and it is assumed that all spins within the cell are perfectly correlated. For example, if the micromagnetic cell is the unit cell of a material like magnetite, which contains 24 magnetic ions, J_{eff} can be estimated by considering the exchange interactions across the faces of the unit cell [44–47]. J_{eff} can also be estimated from a critical magnetic temperature T_c, which, for the example of the classical Heisenberg model on a cubic lattice, follows [48],

$$k_{\mathrm{B}}T_c = 0.24 \times 6J_{\mathrm{eff}} = 0.24 \times 6aA, \tag{8}$$

where a is the cell length (lattice constant) and A is another form of the exchange constant, with units of energy per length. In the continuum limit [49], where spatial variations in $\mathbf{m}_i$ occur on a scale much larger than a and hence it makes sense to think in terms of a field $\mathbf{m}(\mathbf{r})$, the system energy is the product of A and an integral over space of the gradient of $\mathbf{m}(\mathbf{r})$. Experimentally, A can be determined from the analysis of wave motion, i.e. spin waves, in a sample of material [50,51].

The relation $J_{\text{eff}} = aA$ suggests a simple scaling of interactions when varying cell size in micromagnetic simulations. However, it is not so simple, as the larger a is, the less valid the assumption of perfect correlation among spins represented by a single magnetic moment. Finally, factors of 2 abound in the definitions of J, J_{eff} and A depending on context and convention, and so care must be taken in this regard.

3.2. Dipoles, magnetostatics, and shape anisotropy

Unlike quantum-based exchange interactions, dipole interactions are rooted in classical magnetism. The magnetic energy between two magnetic dipoles $\boldsymbol{\mu}_1$ and $\boldsymbol{\mu}_2$ separated by $\mathbf{r}$ is given by [32],

$$E = \frac{\mu_0}{4\pi r^3}\left(\boldsymbol{\mu}_1 \cdot \boldsymbol{\mu}_2 - \frac{3}{r^2}(\boldsymbol{\mu}_1 \cdot \mathbf{r})(\boldsymbol{\mu}_2 \cdot \mathbf{r})\right). \tag{9}$$

In addition to the magnitude of the moments and the distance between them, the magnetic energy depends on their directions relative to each other (first term), just as in Heisenberg exchange, as well as their directions relative to the line joining them (second term). In crystals, this axis is related to the lattice vectors.

Compared to exchange and magnetic anisotropy, the dipole energy is typically orders of magnitude weaker but is long ranged, and can therefore have profound effects on the state of magnetization, and hysteresis loops, for ferromagnetic and ferrimagnetic materials. Ferrimagnetic materials have antiparallel neighbouring spins of unequal magnitude, resulting in a net moment. Owing to cancellation effects, dipole interactions are much less important in the case of antiferromagnets. Two energetically optimal alignments of a pair of magnetic dipoles important for our discussion are shown in Figure 4. In the first case, Figure 4(a), dipole moments are aligned with $\mathbf{r}$. This stable orientation enhances ferromagnetic order. In the case where the moments are perpendicular to $\mathbf{r}$, Figure 4(b), antiparallel orientation is favoured and disrupts long-ranged ferromagnetic order.

In going from an atomic-level description to the micromagnetic one, the inevitable competition between ferromagnetic exchange and dipole interactions limits the range of magnetization correlation, at $T = 0$, to be less than the so-called exchange length [4],

$$l_{\text{ex}} = \sqrt{\frac{2A}{\mu_0 M_{\text{s}}^2}}. \tag{10}$$

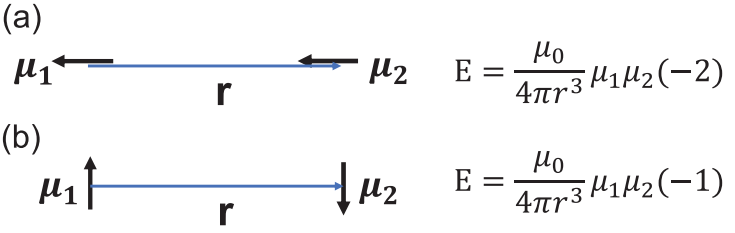

Figure 4. Energetically favourable configurations for (a) parallel (ferromagnetic) and (b) antiparallel (antiferromagnetic) dipole alignments.

As an example, for magnetite, $A = 1 \times 10^{-11}$ J/m [4,45–47,50,52–54] and $M_s = 480$ kA/m [52,55,56], and so micromagnetic simulation cells should be less than $l_{ex} = 8$ nm [4] in length in order to avoid unphysical results.

Once finite micromagnetic cells are used, the point dipoles (Figure 5(a)) only approximately describe the fields generated by the cells (Figure 5(b)). The field at an arbitrary point in space due to a magnetized cell is obtained by integrating the dipolar contributions over the volume of the cell. Through the divergence theorem, the result can be expressed as a surface integral, which, for rectangular prisms, has a closed form solution [57]. The field due to a cell acts on the cell itself (this is the $\mathbf{H}_d$ appearing below in the discussion of shape anisotropy) and has a demagnetizing effect, and is often referred to as *self-demag*. Otherwise, the magnetic field due to a cell is referred to as the *demag* field. The terms *demag* and *self-demag* merely differentiate the effects of magnetostatic interactions.

The shape of a magnetized object may give rise to *shape anisotropy*. The magnetization discontinuity at the surface of a finite-sized ferromagnet leads to effects that can be modelled by a surface layer of magnetic charges or monopoles. The field arising from these surface monopoles is called the demagnetization field $\mathbf{H}_d$. It is a complicated function of the position within magnets of arbitrary shape. However, the Brown-Morrish theorem [56,58]

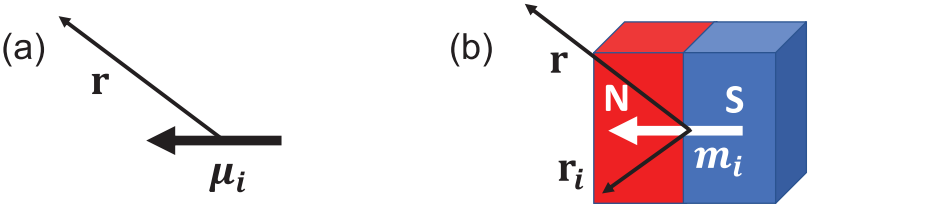

Figure 5. The magnetic field produced by (a) a magnetic point dipole and (b) a bar magnet at distance **r**.

suggests equivalence of an arbitrarily shaped magnetized body with a uniformly magnetized ellipsoid of the same volume. For a uniformly magnetized ellipsoid, $\mathbf{H}_d = -\mathbf{NM}$, where $\mathbf{N}$ is the demagnetizing tensor that depends on the axis lengths of the ellipsoid [32]. In the case of a spheroid, the demagnetization energy density $E = \mu_0 \mathbf{M} \cdot \mathbf{N} \cdot \mathbf{M}/2$ can be written in the form of a uniaxial anisotropy with energy density $K_{\mathrm{sh}} = \frac{\mu_0 M_s^2 (N_\perp - N_{||})}{2}$ [31], where $N_\perp$ and $N_{||}$ are, respectively, demagnetizing factors perpendicular and along the rotational symmetry axis of the spheroid. K_{sh} is positive (easy-axis) for a long, thin (prolate) spheroid. The dimensionless ratio $\mu_0 M_s^2/|K_c|$ estimates the shape anisotropy contribution to the particle's total energy relative to its cubic magnetocrystalline anisotropy. For magnetite spheroids with a ratio as small as 1.2 between semi-axes lengths, effects of cubic anisotropy can be ignored as the uniaxial shape anisotropy is dominant [56]. For an example of calculating the shape anisotropy, see [57,59]. Modeling self-demag with shape anisotropy reduces the computational load in micromagnetic simulations; rather than calculating magnetostatic interactions between all the cells making up a magnetized body, an anisotropy term is simply added to each cell. However, whenever accuracy is preferred to computational speedup, particularly where non-uniform magnetization is expected, the full magnetostatic formalism should be used.

3.3. Other interactions

In addition to the magnetic interactions described above, there are a number of other mostly anisotropic contributions to the energy that can be important for micromagnetic simulations in some cases. These types of terms typically depend on the nature of the crystal symmetry and often have their origin in spin-orbit coupling effects. An example considered in thin-film applications is the fourth-order single-ion uniaxial term of the form [60],

$$\mathcal{H}_{\mathrm{u4}} = -K_4 V (\mathbf{m} \cdot \mathbf{u})^4. \tag{11}$$

Anisotropic terms may also involve interactions between neighboring cells. Systems with single-site uniaxial anisotropy usually have a crystal symmetry that supports the existence of anisotropic exchange in addition to the usual Heisenberg isotropic exchange. This type of exchange term can be written as,

$$\mathcal{H}_{\mathrm{Jz}} = J_z \sum_{<i,j>} \mathbf{m}_{zi} \mathbf{m}_{zj}, \tag{12}$$

and has been shown to impact the structure of MH loops [61]. Systems with exotic magnetic structures called skyrmions [26] have been modelled using micromagnetics where such spin textures are stabilized by the Dzyaloshinskii-Moriya interaction [24,25]. This contribution is allowed by symmetry only for a relatively small set of crystal structures and takes a form that one can think of as a cross-product version of normal exchange,

$$\mathcal{H}_{\mathrm{D}} = \sum_{<i,j>} \mathbf{D_{ij}} \cdot \mathbf{m}_i \times \mathbf{m}_j. \tag{13}$$

These and other less traditional contributions to the energy can usually safely be omitted from most simulations as they are typically small but in some cases they are necessary to explain key phenomena.

4. Dynamics: magnetic torque and the LLG equation

4.1. Torque on a magnetic moment

The torque on the magnetic moment due to a field is $\boldsymbol{\mu} \times \mathbf{B}$, and this lies at the heart of simulating the dynamics of classical magnetic systems. As $\boldsymbol{\mu}$ is associated with angular momentum $\mathbf{S}$ through the gyromagnetic ratio γ via $\boldsymbol{\mu} = -\gamma \mathbf{S}$, and given the fact that the time rate of change of angular momentum is equal to the torque, the time evolution of a magnetic moment is governed by the torque equation,

$$\frac{d\boldsymbol{\mu}}{dt} = -\gamma \boldsymbol{\mu} \times \mathbf{B}, \tag{14}$$

with the result that $\boldsymbol{\mu}$ precesses around $\mathbf{B}$ [32] indefinitely and without decay, maintaining a constant component along $\mathbf{B}$.

In the context of the micromagnetic modelling of materials, Equation 14 applies to each cell, for which $\boldsymbol{\mu} = \mathbf{m} M_s V$ and $\mathbf{B}$ is replaced with $\mu_0 \mathbf{H}_{\mathrm{eff}}$. The result is the Landau-Lifshitz (LL) equation,

$$\frac{d\mathbf{m}}{dt} = -\gamma \mu_0 \mathbf{m} \times \mathbf{H}_{\mathrm{eff}}. \tag{15}$$

In the micromagnetic context, γ is taken to be that of an electron, with $\gamma = eg/2m_e$, where e, m_e and $g \simeq 2$ are the absolute value of an electron's charge, mass and g-factor, respectively. $\mathbf{H}_{\mathrm{eff}}$ represents the sum of different interactions as,

$$\mathbf{H}_{\mathrm{eff}} = \mathbf{H}_{\mathrm{Zeeman}} + \mathbf{H}_{\mathrm{ani}} + \mathbf{H}_{\mathrm{magnetostatic}} + \mathbf{H}, \tag{16}$$

where the field contribution at the i^{th} cell can be calculated via the derivative of the appropriate energy with respect to magnetization, e.g., for anisotropy,

$$\mathbf{H}_{\text{ani}} = -\frac{1}{\mu_0 M_s V}\frac{\partial \mathcal{H}_{\text{ani}}}{\partial \mathbf{m}_i} = -\frac{1}{\mu_0 M_s V}\frac{\partial}{\partial \mathbf{m}_i}\left(-KV(\mathbf{m}_i \cdot \mathbf{u}_i)^2\right) = \frac{2K}{\mu_0 M_s}(\mathbf{m}_i \cdot \mathbf{u}_i)\mathbf{u}_i, \tag{17}$$

and exchange, where we assume that $V = a^3$ and recall that $J_{\text{eff}} = aA$,

$$\mathbf{H}_{\text{ex}} = -\frac{1}{\mu_0 M_s V}\frac{\partial}{\partial \mathbf{m}_i}\left(-\frac{J_{\text{eff}}}{2}\sum_j \sum_{k\in N_j} \mathbf{m}_j \cdot \mathbf{m}_k\right) = \frac{A}{\mu_0 M_s a^2}\sum_{j\in N_i} \mathbf{m}_j, \tag{18}$$

where $j \in N_i$ signifies that the index j runs over the neighbouring cells of cell i.

4.2. The Landau-Lifshitz-Gilbert equation

As with the simple torque (Equation 14), the LL (Equation 15) implies that the magnetization vector precesses around the effective field forever. They both neglect the decay of the magnetic moment's precession from dissipation effects and the resulting eventual alignment with the effective field direction. Attributing this decay to various factors, such as coupling of magnetic moments to the lattice, lattice disorder, defects, impurities, etc., Gilbert [62] suggested adding a damping term to the effective field,

$$\mathbf{H}_{\text{eff}} \longrightarrow \mathbf{H}_{\text{eff}} - \eta\frac{d\mathbf{M}}{dt}, \tag{19}$$

where the damping coefficient $\eta = \alpha/(\mu_0\gamma M_{\text{s}})$ depends on a dimensionless phenomenological damping parameter α, which results from both intrinsic properties of the material and extrinsic effects (e.g. defects) [62–67]. Incorporating damping results in the Landau-Lifshitz-Gilbert (LLG) equation,

$$\frac{d\mathbf{m}}{dt} = -\left(\frac{\gamma_1}{1+\alpha^2}\right)\mathbf{m} \times \mathbf{H}_{\text{eff}} - \left(\frac{\gamma_1 \alpha}{1+\alpha^2}\right)\mathbf{m} \times (\mathbf{m} \times \mathbf{H}_{\text{eff}}), \tag{20}$$

where $\gamma_1 = \mu_0\gamma$.

To study systems at finite temperature, a stochastic term based on the fluctuation-dissipation theorem [68] is added to the effective field,

$$\mathbf{H}_{\text{thermal}} = \mathbf{\Gamma}\sqrt{\frac{2\alpha k_{\text{B}} T}{V\mu_0\gamma_1 M_{\text{s}}\Delta t}}, \tag{21}$$

where k_B is the Boltzmann constant and $\mathbf{\Gamma} = \mathbf{\Gamma}(t)$ is a random vector with Cartesian components drawn at each time step during the numerical solution from a Gaussian distribution with zero mean and unit variance. Given the dependence of $\mathbf{H}_{\text{thermal}}$ on V and the time step Δt of the numerical solver, one needs to be careful in choosing an appropriate Δt, particularly for small V. With the addition of $\mathbf{H}_{\text{thermal}}$, the resulting equation is often called the stochastic LLG equation, sLLG. We note that there are slight variations in how precisely the stochastic term enters the equation [69,70]. The sLLG equation can be used to study the magnetization dynamics for low to high damping limits ($\alpha \sim 0.001 - 1$). A variety of numerical techniques have been successfully employed to solve the LLG and sLLG [71] equations, and numerous software packages are available: OOMMF [72], Vinamax [73], MuMax [74,75], and finite element codes [49,76–79] with bright prospects for the future [80].

Traditional micromagnetics is based on the assumption that the magnitude of the magnetization vector remains constant. An extension of the LLG equation, the Landau-Lifshitz-Bloch equation, which incorporates a phenomenological formulation of the effects of thermal fluctuations on $|\mathbf{m}|$, has been demonstrated to provide a good description for a number of applications [81,82].

5. Scaling

Omitted from our discussion thus far is how simulation results are affected if the cell size is changed, or rather, how to scale parameters like A and K so that results are independent of a. The difficulty is made apparent when considering that different contributions to $\mathbf{H}_{\text{eff}}$ scale differently with a: e.g. $\mathbf{H}_{\text{ani}} \propto a^0$, $\mathbf{H}_{\text{ex}} \propto a^{-2}$ and $\mathbf{H}_{\text{thermal}} \propto a^{-3/2}$.

Simulating a sample of magnetic material using bigger but fewer cells, i.e. coarse-graining, is desirable in order to decrease the number of calculations and hence simulation time. This is particularly useful for the study of larger systems. Moreover, considering Equation 21, using bigger simulation cells allows for a longer integration time step, again resulting in faster calculations. However, simply using larger cells, especially approaching or exceeding that of the nominal exchange length, carries the risk of obscuring the essential physics of a problem of interest. Scaling the magnetic parameters properly with cell size is essential, and not trivial.

Among the different approaches for coarse-graining [83–90], we here cast the problem in terms of the theoretically appealing renormalization group (RG) approach taken by Grinstein and Koch [86]. Let us assume that for a simulation carried out with cell size a_0, magnetic parameters A_0 and K_0, and field strength H_0, we obtain the resulting magnetization M_0. If we then increase the cell size to $a_b = ba_0$ ($b > 1$), we need to carry out simulations with

coarse-grained parameters $A(b)$ and $K(b)$, and field $H(b)$ all chosen in such a way so that we can map the resulting $M(b)$ to M_0. In Ref. [27], we modified and applied the approach in Ref. [86], arriving at a set of relations between coarse-grained and original quantities in the limit of strong exchange relative to anisotropy and Zeeman terms,

$$\begin{aligned} A(b) &= \zeta(b) \times A_0 \\ K(b) &= \zeta(b)^3 \times K_0 \\ H(b) &= \zeta(b) \times H_0 \\ M_0 &= \delta\zeta(b)M(b) + (1-\delta)M(b), \end{aligned} \tag{22}$$

where the scaling factor $\zeta(b) = t/b + 1 - t$, with $t = T/T_c$, with T_c being the Curie temperature. The parameter $\delta = 0.511$ was obtained from a one-parameter fit of $M_0(T)$ computed without any scaling.

The above approach was applied in Ref. [27] to calculate hysteresis loops of a magnetite nanorod modelled with exchange and uniaxial anisotropy of dimensions $8a_0 \times 24a_0 \times 56a_0$, where $a_0 = 0.839$ nm is the size of the crystallographic unit cell. In Figure 6(a), the results for $b = 1$ involved simulating 10,752 micromagnetic cells, taking months to complete. The rest of the curves show progressive departure from the $b = 1$ result when cell size is increased without scaling any of the other quantities. In Figure 6(b), the results show much better agreement when the scaling given by Equation 22 is used. This methodology was further developed to include magnetostatic interactions [28], and with the speed-up provided by coarse-graining, was applied to simulating clusters of interacting nanoparticles with complex internal structure [29]. Despite being able to find a single effective 'macrospin' description of an entire nanoparticle composed of several nanorods, we found that the macrospin approximation failed when the nanoparticles were very close to each other.

More recently, Schrefl et al. [90] produced a method of scaling interaction parameters by integrating spin-wave fluctuations smaller than the cell size. The authors make the case that this method should have a broader range of applicability than RG approaches, e.g. for materials with large anisotropies and high fields.

6. Coupling magnetic dynamics with particle motion

Our discussion up until now has focused exclusively on magnetization dynamics, neglecting motion of or within the magnetized body. However, there is growing interest in simulating systems where magnetic and mechanical degrees of freedom are coupled, both in atomic and colloidal systems.

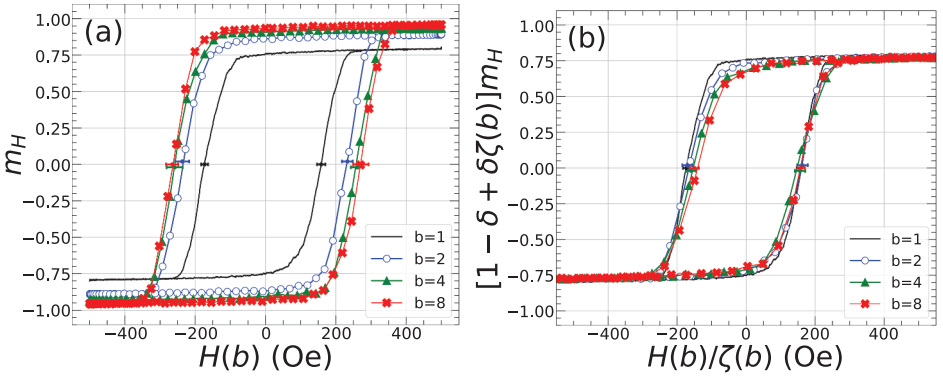

Figure 6. Application of RG coarse graining to nanorod MH loops at $T = 310$ K and SR $= 2.5$ Oe/ns. (a) Changing cell length ($a = ba_0$) without changing magnetic parameters. (b) Quantities are scaled according to Equation 22. Figures adapted from Ref. [27].

For atomic systems, the micromagnetic equations of motion apply, but now with a cell's magnetic moment $\mathbf{m}M_sV$ replaced with an atomic magnetic moment $\boldsymbol{\mu}$ [91]. In addition to dipolar forces, forces on atoms arise from, e.g. the distance dependence of the exchange coupling between atoms. Spin dynamics-molecular dynamics (SPMD) simulations have already been used in several studies [34] and have been implemented in available codes such as *Spilady* [92] and within the popular MD code LAMMPS through the SPIN package [93,94]. The authors of such codes develop and use the necessary numerical framework to properly integrate the equations of motion for the translational and spin degrees of freedom, using, for example, a Trotter-expansion-based method that conserves the spin vector magnitude [34,95] or implicit variants [94].

Examples of the use of SPMD include the study of phase transitions [96,97], effects of spin-orbit coupling [98], magnetocrystalline anisotropy and anisotropic magnetostriction [99], understanding mechanisms of (Gilbert) damping [100], electron transport across nanocontacts [101], and iron nanoclusters [102].

For magnetic nanoparticles, the basic ideas behind micromagnetics return, now with the nanoparticle represented by a single magnetization vector. The anisotropy axis is fixed to the nanoparticle, which is modelled as a rigid body (RB) that can now undergo rotations and translations. In this case, the magnetization (once again described by **m**) and orientation of the RB (described by the anisotropy axis vector **u**) are coupled but evolve separately. When the so-called Néel relaxation time $\tau_N = \tau_0 \exp KV/k_BT$ is much faster than the rotational relaxation time $\tau_B = 3\eta V_H/k_BT$ (also referred to as the Brownian relaxation time), we return to the Stoner–Wolhfarth model. Here V refers to the magnetic volume, while V_H refers to the hydrodynamic (or total) volume. A nanoparticle with a magnetic core surrounded by a non-magnetic

shell would have $V_H > V$. Understanding relative contributions of Brownian and Néel relaxation is important for biomedical application of magnetic nanoparticles [103,104]. In the limit of high anisotropy, **m** may be regarded as being fixed along **u** and the magnetization dynamics are dictated by particle rotation.

Examples of studies that couple rotational and magnetization dynamics of magnetic nanoparticles (MNPs) include calculating specific absorption rates of iron NPs with cubic anisotropy distributed in a viscous liquid [105,106]; alignment of suspended MNPs to external fields with biomedical applications [107,108]; magnetic and mechanical contributions to MNP heating [109–111]; the role of particle size on relative importance of Néel and Brownian (at large sizes, the magnetic moment is locked with the particle axis) [112]; the effect of interparticle interactions on the magnetization dynamics and energy dissipation rates [113]; and magnetization response under a pulsed field [114].

6.1. Coupling of nanoparticle rotational and magnetization dynamics

We now review the equations governing magnetization dynamics for a particle that is free to rotate [35,115–118], the development of which can be found in Refs. [35] and [117]. Consider a spherical magnetic nanoparticle with a magnetic uniaxial anisotropy axis fixed rigidly to it. As before, this axis lies along the unit vector **u** and the energy associated with the anisotropy is given by Equation 2. The anisotropic interaction can again be described by an effective anisotropy field (given by Equation 17). This field gives rise to a torque on the magnetic moment, a torque due to the rest of the nanoparticle (the RB), given by,

$$\boldsymbol{\tau}_m = \boldsymbol{\mu} \times \mathbf{B} = \mu_0 M_s V \mathbf{m} \times \mathbf{H}_{\text{ani}} = 2KV(\mathbf{m} \cdot \mathbf{u})\mathbf{m} \times \mathbf{u}. \tag{23}$$

There will be an equal and opposite torque on the body due to the magnetic moment. Recalling that $\mathbf{S} = -\frac{\boldsymbol{\mu}}{\gamma_e} = -\frac{1}{\gamma_e} M_s V \mathbf{m}$ and that $\frac{d\mathbf{S}}{dt} = \boldsymbol{\tau}_m$, we write Equation 15 as,

$$\frac{d\mathbf{m}}{dt} = -\mu_0 \gamma_e \mathbf{m} \times \mathbf{H}_{\text{ani}} = -\gamma_e \frac{2K}{M_s} (\mathbf{m} \cdot \mathbf{n})\mathbf{m} \times \mathbf{u}, \tag{24}$$

and a corresponding equation for the angular momentum of the RB as,

$$\frac{d\mathbf{L}}{dt} = -\boldsymbol{\tau}_m = -2KV(\mathbf{m} \cdot \mathbf{n})\mathbf{m} \times \mathbf{u}, \tag{25}$$

that ensures that $\mathbf{J} = \mathbf{L} + \mathbf{S}$ is constant. If an external field $\mathbf{H}_{\text{ext}}$ is present, then Equation 25 remains unchanged, and Equation 24 becomes,

$$\frac{d\mathbf{m}}{dt} = -\mu_0 \gamma_e \mathbf{m} \times (\mathbf{H}_{\text{ani}} + \mathbf{H}_{\text{ext}}) . \tag{26}$$

Equations 25 and 24 or 26 conserve energy, and are useful for checking implementations of numerical integration algorithms.

As with pure micromagentics, we would like to consider the case that includes magnetic damping through the loss of magnetic energy to microscopic degrees of freedom. In this case, there is a drag torque that will allow the magnetization to align with the anisotropy axis instead of continually precessing. A fundamental assumption is that this torque is due to the body, and so there must be a compensating torque due to the magnetization on the body. The equations of motion for Langevin dynamics are [35,117],

$$\frac{d\mathbf{m}}{dt} = \mathbf{h}_D \times \mathbf{m}, \tag{27}$$

with

$$\mathbf{h}_D = \boldsymbol{\omega} + \frac{\mu_0 \gamma_e}{1+\alpha^2} \left\{ \left(\mathbf{H}_{\text{eff}} - \frac{\boldsymbol{\omega}}{\gamma} \right) + \alpha \mathbf{m} \times \left(\mathbf{H}_{\text{eff}} - \frac{\boldsymbol{\omega}}{\gamma} \right) \right\}, \tag{28}$$

$$\frac{d\mathbf{u}}{dt} = \boldsymbol{\omega} \times \mathbf{u}, \tag{29}$$

and

$$\Theta \frac{d\boldsymbol{\omega}}{dt} = \frac{M_s V}{\gamma_e} \frac{d\mathbf{m}}{dt} + \mu_0 M_s V \mathbf{m} \times (\mathbf{H}_{\text{ext}} + \boldsymbol{\zeta}) - \xi \boldsymbol{\omega} + \boldsymbol{\epsilon}, \tag{30}$$

where $\boldsymbol{\omega}$ is the angular velocity of the body, Θ is the moment of inertia, and $\boldsymbol{\tau}_{\text{fluid}} = -\xi\boldsymbol{\omega} + \boldsymbol{\epsilon}$ is the torque due to the fluid. The factors α and $\xi = 6\eta V_H$, with η being the viscosity, are magnetic and rotational damping constants, respectively, while $\boldsymbol{\zeta}$ and $\boldsymbol{\epsilon}$ are stochastic vectors with components drawn from normal distributions with zero mean and variances given by,

$$\sigma_\zeta^2 = \frac{2\,\alpha\, k_B T}{\mu_0^2 M_s V \gamma_e \Delta t} \tag{31}$$

and

$$\sigma_\epsilon^2 = \frac{2\,\xi\,k_B T}{\Delta t}, \tag{32}$$

respectively, with Δt being the simulation time step. The effective field is given by,

$$\mathbf{H}_{\text{eff}} = \mathbf{H}_{\text{ext}} + \mathbf{H}_K + \boldsymbol{\zeta}. \tag{33}$$

For sufficiently small particles, Θ becomes negligible, and Equation 30 can be solved algebraically for $\boldsymbol{\omega}$ [35,117],

$$\boldsymbol{\omega} = \frac{1}{\xi}\left(\frac{M_s V}{\gamma_e}\mathbf{h}_D \times \mathbf{m} + \mu_0 M_s V \mathbf{m} \times (\mathbf{H}_{\text{ext}} + \boldsymbol{\zeta}) + \boldsymbol{\epsilon}\right). \tag{34}$$

The inclusion of $\boldsymbol{\zeta}$ in Equations 30 and 34 is subject to interpretation [119]. If the thermal stochastic term affecting $\mathbf{m}$ arises only from torques internal to the nanoparticle, then $\boldsymbol{\zeta}$ should not appear in Equation 30 (i.e. not added to $\mathbf{H}_{\text{ext}}$ within the parentheses on the right hand side of the equation). This can be most easily understood by considering that angular momentum changes only from external torques,

$$\begin{aligned} \frac{d\mathbf{J}}{dt} &= \tau_{\text{external}} \\ \frac{d(\mathbf{L}+\mathbf{S})}{dt} &= \mu_0 M_s V \mathbf{m} \times \mathbf{H}_{\text{ext}} - \xi\boldsymbol{\omega} + \epsilon \\ \Theta\frac{d\boldsymbol{\omega}}{dt} &= \frac{M_s V}{\gamma_e}\frac{d\mathbf{m}}{dt} + \mu_0 M_s V \mathbf{m} \times \mathbf{H}_{\text{ext}} - \xi\boldsymbol{\omega} + \epsilon. \end{aligned} \tag{35}$$

Regardless of the interpretation, i.e. whether or not $\boldsymbol{\zeta}$ is explicitly included in Equations 30 and 34, the numerical example below confirms that both approaches yield indistiguishable results when the ratio $\frac{M_s V}{\xi\gamma_e}$ [117] is small [119].

In [117], Usadel developed the equations of motion for the case where $\mathbf{m}$ maintains alignment with $\mathbf{u}$, i.e., $\mathbf{m} = \mathbf{u}$, in the high K limit (and where thermal switching does not take place). This limit, or rigid dipole (RD) model,

can be understood again by considering the change in angular momentum,

$$\begin{aligned}\frac{d\mathbf{J}}{dt} &= \Theta\frac{d\boldsymbol{\omega}}{dt} - \frac{M_s V}{\gamma_e}\frac{d\mathbf{m}}{dt} \\ &= \Theta\frac{d\boldsymbol{\omega}}{dt} - \frac{M_s V}{\gamma_e}\frac{d\mathbf{u}}{dt} \\ &= \Theta\frac{d\boldsymbol{\omega}}{dt} - \frac{M_s V}{\gamma_e}\boldsymbol{\omega}\times\mathbf{u} \\ &= \tau_{\text{ext}},\end{aligned} \tag{36}$$

or

$$\Theta\frac{d\boldsymbol{\omega}}{dt} = \frac{M_s V}{\gamma_e}\boldsymbol{\omega}\times\mathbf{u} + M_s V\mathbf{u}\times(\mathbf{B}_{\text{ext}} + \boldsymbol{\zeta}) + \boldsymbol{\tau}_{\text{fluid}}, \tag{37}$$

where once again we note that the inclusion of $\boldsymbol{\zeta}$ as causing an external torque is a matter of interpretation (and can be omitted). From this, we see that, apart from $\boldsymbol{\tau}_{\text{fluid}}$ and a torque stemming from $\boldsymbol{\zeta}$, the RD feels a torque,

$$\frac{M_s V}{\gamma_e}\boldsymbol{\omega}\times\mathbf{u} + M_s V\mathbf{u}\times\mathbf{B}_{\text{ext}} = M_s V\mathbf{u}\times\left(\mathbf{B}_{\text{ext}} - \frac{\boldsymbol{\omega}}{\gamma_e}\right), \tag{38}$$

and not simply $M_s V\mathbf{u}\times\mathbf{B}_{\text{ext}}$.

If we are only interested in tracking the magnetization in the Brownian ($\Theta = 0$) limit, the equations simplify to [112,117],

$$\frac{d\mathbf{m}}{dt} = \mathbf{h}_{\text{RD}}\times\mathbf{m}, \tag{39}$$

with

$$\mathbf{h}_{\text{RD}} = \frac{1}{1 - \frac{M_s V}{\xi\gamma_e}}\frac{1}{\xi}\left(\boldsymbol{\epsilon} + M_s V\mathbf{m}\times\mathbf{B}_{\text{ext}}\right), \tag{40}$$

where, again, the term $M_s V/(\xi\gamma_e)$ is often negligible, and Usadel omits it. In a similar spirit, in Ref. [117], Usadel argues that $\boldsymbol{\zeta}$ in Equation 37 is negligible to first order in $M_s V/(\xi\gamma_e)$ and omitted it from Equation 40.

6.2. Example

As an illustration of the above methods, in Figure 7 we show the results of applying Usadel's formalism to study the effects of Brownian rotation on hysteresis for the magnetite nanorod introduced earlier in section 5 [27], modelled as a sphere of the same volume as the nanorod, at various viscosities.

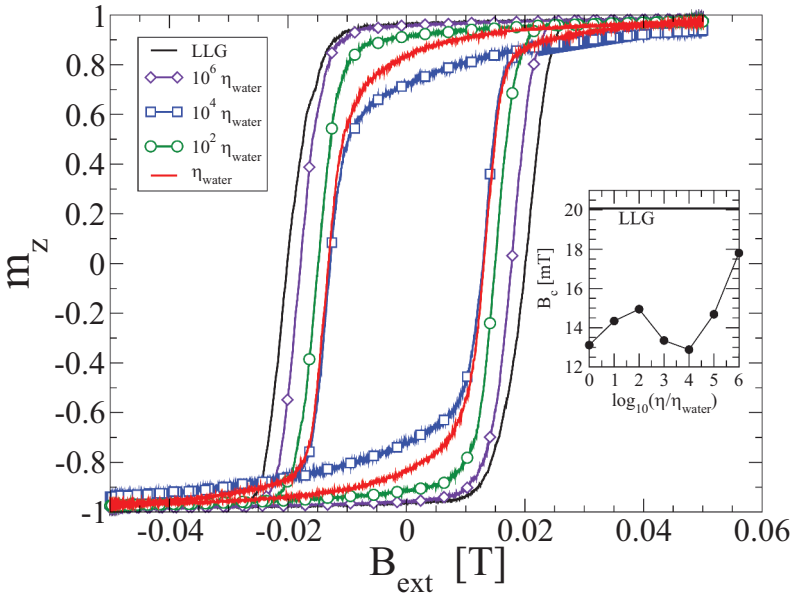

Figure 7. *MH* loops for a magnetic nanoparticle at $T = 310$ K in a fluid at several viscosities, given in terms of the viscosity of water, calculated according Equations 27, 28, 29 and 35 (with $\Theta = 0$, and so solved algebraically for ω), compared with a purely micromagnetic calculation (no rotation of the nanoparticle allowed), Equation 20 (black curve, no symbols).

For the external field frequency of $f = 125$ kHz, Brownian motion significantly reduces the loop area, relative to purely micromagnetic modelling, once the viscosity is reduced (from infinity) to $10^3\eta_{\text{water}}$, which is a reasonable estimate for kidney tissue [120]. We also see a non-monotonic dependence of the loop area, as partially quantified by the plot of the coercive field as a function of T in the inset of Figure 7. This interesting feature warrants further study but is similar to Usadel's result that there is an optimal size for absorbed power at fixed field strength, frequency and T.

The parameters we use in the example are as follows: $T = 310$ K $M_s = 480 \times 10^3$ A/m, $K = 10^4$ J/m^3, $V = 6.331625 \times 10^{-24}$ m^3 which is $(18.5\text{ nm})^3$, $\rho = 7874$ kg/m^3, $\alpha = 0.1$, $B_{\text{max}} = 50$ mT, $B_z(T) = B_{\text{max}} \cos(2\pi ft)$, $\eta_{\text{water}} = 10^{-3}$ Pa.s. The system is equilibrated for 100 loops, and then data are collected and averaged over 1000 loops. We use Equation 34, both with and without ζ on the right hand side. For $\eta \geq \eta_{\text{water}}$, the ratio $\frac{M_s V}{\xi\gamma_e} \leq 4.543 \times 10^{-4}$, and the resulting hysteresis loops with and without ζ are indistinguishable. The results are plotted without ζ in Equation 34. The stochastic equations of motions are integrated using Heun's solver [121,122] with a time step of 1 ps.

As a test on the inclusion of ζ in Equation 34, we calculate the heat capacity for the same model nanoparticle. Nominally, $\Theta = 2.627 \times 10^{-36}$ kg.m^2, as obtained from the moment of inertia of a sphere $\frac{2}{5}(\rho V)\left(\frac{3V}{4\pi}\right)^{\frac{2}{3}}$. However, we

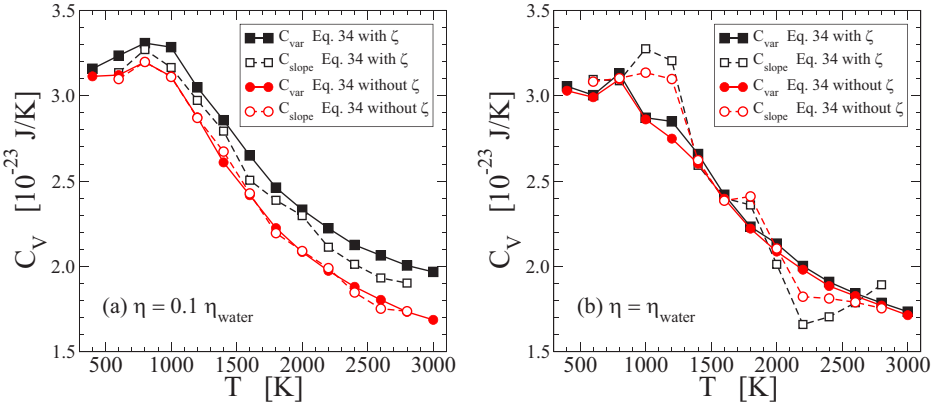

Figure 8. Heat capacity comparisons in the high damping limit with (a) $\eta = \eta_{\text{water}}/10$. C_{var} (filled squares) and C_{slope} (open squares) obtained using Equation 34 show a systematic deviation from each other. Removing $\boldsymbol{\zeta}$ from Equation 34, such that $\boldsymbol{\zeta}$ provides no external torque and enters the equations of motion only through Equation 33, yields C_{var} (filled circles) and C_{slope} (open circles) that are consistent with each other. Panel (b) shows results at a higher viscosity, $\eta = \eta_{\text{water}}$, with greater consistency between including and not including $\boldsymbol{\zeta}$ in Equation 34.

set $\Theta = 0$ since we use Equation 34, thus neglecting the rotational kinetic energy and its contribution to the heat capacity. In Figure 8(a), we plot for $\eta = \eta_{\text{water}}/10$ and $B_{\text{ext}} = \mu_0 H_{\text{ext}} = 4$ mT the heat capacity obtained from fluctuations in the energy,

$$C_{\text{var}} = \frac{<E^2> - <E>^2}{k_B T^2}, \tag{41}$$

with filled symbols, and from the derivative with respect to T,

$$C_{\text{slope}} = \frac{d<E>}{dT}, \tag{42}$$

with open symbols. The results using Equation 34 (squares) deviate from each other, while omitting the explicit appearance of $\boldsymbol{\zeta}$ on the right-hand-side of Equation 34 yields consistent curves. For $\eta = \eta_{\text{water}}$, shown in Figure 8(b), there is greater consistency between data sets. While our example is not particularly physically meaningful, given the T range employed, it does serve as a note of caution when modelling the effects of T through the inclusion of $\boldsymbol{\zeta}$ in Equations 30 and 34, or at least as an encouragement to test for consistency in one's results when including $\boldsymbol{\zeta}$ in Equations 30 and 34. The heat capacity simulations are performed using 2×10^8 equilibration time steps followed by 8×10^8 steps over which statistics are gathered. The simple centred difference scheme is used to calculate C_{slope} from $<E(T)>$.

7. Concluding remarks

In writing this review, we have covered the micromagnetics background that two of us would have greatly benefited from knowing prior to starting computational research on magnetic nanoparticle hyperthermia, having come from an MD simulation background. We have learned that the application of micromagnetics to study problems where temperature and process rates are important can be challenging when coarse graining is required to bridge different length scales. We have shown in our previous works, as highlighted in section 5, that scaling methods taken from fundamental concepts in renormalization group theory are useful for this purpose in the study of magnetic hyperthermia. Using this or alternative scaling approach to study other problems where thermodynamics plays a key role warrants consideration.

MD simulations have grown immensely in applicability and use since their humble beginnings with hard spheres [123] and now are used extensively in many research areas within, e.g. biochemistry, chemical physics, and materials engineering. There are several well supported, well documented and flexible computer codes and associated tools for system setup and analysis. Several books, now classics, have been written to bring students up to speed on how to write or properly use simulation codes, analyze data and implement advanced techniques based on statistical mechanics.

We are very pleased to see similar development in micromagnetic simulations, and expect to see continued growth in the application or consideration of micromagnetism as available codes become more accessible and research areas broaden into biomedical areas. Notable is the inclusion of SPMD in the popular MD code LAMMPS [93], which has facilitated research where lattice motions couple with magnetization dynamics. We would encourage similar inclusion of magnetization dynamics within colloidal particles as a boon to the magnetic nanoparticle community, including in new areas such as magnetically controlled nanoswimmers [124].

Funding

The work was supported by the Natural Science and Engineering Research Council of Canada [RGPIN-2016-04499 and RGPIN-2017-05569].

Acknowledgments

We thank K. D. Usadel, J. Tranchida and M. Karttunen for pleasant and fruitful discussions. MLP and ISV thank the Natural Sciences and Engineering Research Council (Canada) for funding.

Disclosure statement

No potential conflict of interest was reported by the author(s).

References

[1] Wilson KG. Problems in physics with many scales of length. Sci Am. 1979;241:158–179. doi: 10.1038/scientificamerican0879-158

[2] Ptuskin VS, Moskalenko IV, Jones FC, et al. Dissipation of magnetohydrodynamic waves on energetic particles: impact on interstellar turbulence and cosmic-ray transport. Astrophysical J. 2006;642:902. doi: 10.1086/501117

[3] Žutić I, Fabian J, Sarma SD. Spintronics: fundamentals and applications. Rev Mod Phys. 2004;76:323. doi: 10.1103/RevModPhys.76.323

[4] Abo GS, Hong YK, Park J, et al. Definition of magnetic exchange length. IEEE Trans Magn. 2013;49:4937–4939. doi: 10.1109/TMAG.2013.2258028

[5] Kittel C. Theory of the dispersion of magnetic permeability in ferromagnetic materials at microwave frequencies. Phys Rev. 1946;70:281. doi: 10.1103/PhysRev.70.281

[6] Brown W Jr. Micromagnetics. New York: Wiley Interscience; 1963.

[7] Brown WF Jr. Some magnetostatic and micromagnetic properties of the infinite rectangular bar. J Appl Phys. 1964;35:2102–2106. doi: 10.1063/1.1702798

[8] Suess D, Fidler J, Schrefl T. Micromagnetic simulation of magnetic materials. Handb Magnetic Mater. 2006;16:41–125.

[9] Plumer ML, Van Ek J, Weller D. The physics of ultra-high-density magnetic recording. Vol.41. Berlin Heidelberg: Springer-Verlag; 2001. doi: 10.1007/978-3-642-56657-8

[10] Xue J, Victora RH. Micromagnetic predictions for thermally assisted reversal over long time scales. Appl Phys Lett. 2000;77:3432–3434. doi: 10.1063/1.1331094

[11] Zhu JG, Li H. Understanding signal and noise in heat assisted magnetic recording. IEEE Trans Magn. 2013;49:765–772. doi: 10.1109/TMAG.2012.2231855

[12] Zhu JG, Bertram HN. Micromagnetic studies of thin metallic films (invited). J Appl Phys. 1988;63:3248–3253. doi: 10.1063/1.341167

[13] Covington M, Crawford T, Parker G. Time-resolved measurement of propagating spin waves in ferromagnetic thin films. Phys Rev Lett. 2002;89:237202. doi: 10.1103/PhysRevLett.89.237202

[14] Schrefl T, Fidler J, Kirk K, et al. Domain structures and switching mechanisms in patterned magnetic elements. J Magn Magn Mater. 1997;175:193–204. doi: 10.1016/S0304-8853(97)00156-X

[15] Heyderman LJ, Nolting F, Backes D, et al. Magnetization reversal in cobalt antidot arrays. Phys Rev B. 2006;73:214429. doi: 10.1103/PhysRevB.73.214429

[16] Leliaert J, Van De Wiele B, Vansteenkiste A, et al. A numerical approach to incorporate intrinsic material defects in micromagnetic simulations. J Appl Phys. 2014;115. doi: 10.1063/1.4854956

[17] Gypens P, Leo N, Menniti M, et al. Thermoplasmonic nanomagnetic logic gates. Phys Rev Appl. 2022;18. doi: 10.1103/PhysRevApplied.18.024014

[18] Tejo F, Fernandez-Roldan JA, Guslienko KY, et al. Giant supermagnonic Bloch point velocities in cylindrical ferromagnetic nanowires. Nanoscale. 2024;16:10737–10744. doi: 10.1039/D3NR05013K

[19] Thiesen B, Jordan A. Clinical applications of magnetic nanoparticles for hyperthermia. Int J Hyperth. 2008;24:467–474. doi: 10.1080/02656730802104757

[20] Vallejo-Fernandez G, Whear O, Roca A, et al. Mechanisms of hyperthermia in magnetic nanoparticles. J Phys D Appl Phys. 2013;46:312001. doi: 10.1088/0022-3727/46/31/312001

[21] Salunkhe AB, Khot VM, Pawar S. Magnetic hyperthermia with magnetic nanoparticles: a status review. Curr Top Med Chem. 2014;14:572–594. doi: 10.2174/1568026614666140118203550

[22] Périgo EA, Hemery G, Sandre O, et al. Fundamentals and advances in magnetic hyperthermia. Appl Phys Rev. 2015;2:041302. doi: 10.1063/1.4935688
[23] Torche P, Munoz-Menendez C, Serantes D, et al. Thermodynamics of interacting magnetic nanoparticles. Phys Rev B. 2020;101:224429. doi: 10.1103/PhysRevB.101.224429
[24] Mochizuki M. Spin-wave modes and their intense excitation effects in skyrmion crystals. Phys Rev Lett. 2012;108:017601. doi: 10.1103/PhysRevLett.108.017601
[25] Lin SZ, Batista CD, Saxena A. Internal modes of a skyrmion in the ferromagnetic state of chiral magnets. Phys Rev B. 2014;89:024415. doi: 10.1103/PhysRevB.89.024415
[26] Back C, Cros V, Ebert H, et al. The 2020 skyrmionics roadmap. J Phys D Appl Phys. 2020;53:363001. doi: 10.1088/1361-6463/ab8418
[27] Behbahani R, Plumer ML, Saika-Voivod I. Coarse-graining in micromagnetic simulations of dynamic hysteresis loops. J Phys Condens Matter. 2020;32:35LT01. doi: 10.1088/1361-648X/ab8c8d
[28] Behbahani R, Plumer ML, Saika-Voivod I. Multiscale modelling of magnetostatic effects on magnetic nanoparticles with application to hyperthermia. J Phys Condens Matter. 2021;33:215801. doi: 10.1088/1361-648X/abe649
[29] Behbahani R, Plumer ML, Saika-Voivod I. Micromagnetic simulations of clusters of nanoparticles with internal structure: application to magnetic hyperthermia. Phys Rev Appl. 2022;18:034034. doi: 10.1103/PhysRevApplied.18.034034
[30] Dennis CL, Jackson AJ, Borchers JA, et al. Nearly complete regression of tumors via collective behavior of magnetic nanoparticles in hyperthermia. Nanotechnology. 2009;20:395103. doi: 10.1088/0957-4484/20/39/395103
[31] Cullity BD, Graham CD. Introduction to magnetic materials. Hoboken, NJ: John Wiley & Sons; 2009.
[32] Blundell S. Magnetism in condensed matter. (NY): Oxford University Press Inc.; 2009.
[33] Spaldin N. Magnetic materials: fundamentals and device applications. Cambridge: Cambridge University Press; 2003.
[34] Beaujouan D, Thibaudeau P, Barreteau C. Anisotropic magnetic molecular dynamics of cobalt nanowires. Phys Rev B. 2012;86:174409. doi: 10.1103/PhysRevB.86.174409
[35] Usadel KD, Usadel C. Dynamics of magnetic single domain particles embedded in a viscous liquid. J Appl Phys. 2015;118:234303. doi: 10.1063/1.4937919
[36] Hergt R, Dutz S, Röder M. Effects of size distribution on hysteresis losses of magnetic nanoparticles for hyperthermia. J Phys Condens Matter. 2008;20:385214. doi: 10.1088/0953-8984/20/38/385214
[37] Eggeman AS, Majetich SA, Farrell D, et al. Size and concentration effects on high frequency hysteresis of iron oxide nanoparticles. IEEE Trans Magn. 2007;43:2451–2453. doi: 10.1109/TMAG.2007.894127
[38] Mehdaoui B, Tan RP, Meffre A, et al. Increase of magnetic hyperthermia efficiency due to dipolar interactions in low-anisotropy magnetic nanoparticles: theoretical and experimental results. Phys Rev B. 2013;87:174419. doi: 10.1103/PhysRevB.87.174419
[39] Labaye Y, Crisan O, Berger L, et al. Surface anisotropy in ferromagnetic nanoparticles. J Appl Phys. 2002;91:8715–8717. doi: 10.1063/1.1456419
[40] Usov NA, Grebenshchikov YB. Hysteresis loops of an assembly of superparamagnetic nanoparticles with uniaxial anisotropy. J Appl Phys. 2009;106:023917. doi: 10.1063/1.3173280
[41] Fal TJ, Mercer JI, Leblanc MD, et al. Kinetic monte carlo approach to modeling thermal decay in perpendicular recording media. Phys Rev B. 2013;87:064405. doi: 10.1103/PhysRevB.87.064405
[42] Ashcroft NW, Mermin ND. Solid state physics. Fort Worth: Harcourt; 1976.
[43] Kittel C, McEuen P. Introduction to solid state physics. Hoboken, NJ: John Wiley & Sons; 2018.

[44] Bercoff PG, Bertorello HR. Exchange constants and transfer integrals of spinel ferrites. J Magn Magn Mater. 1997;169:314–322. doi: 10.1016/S0304-8853(96)00748-2
[45] Srivastava CM, Srinivasan G, Nanadikar NG. Exchange constants in spinel ferrites. Phys Rev B. 1979;19:499. doi: 10.1103/PhysRevB.19.499
[46] Uhl M, Siberchicot B. A first-principles study of exchange integrals in magnetite. J Phys Condens Matter. 1995;7:4227. doi: 10.1088/0953-8984/7/22/006
[47] Glasser ML, Milford FJ. Spin wave spectra of magnetite. Phys Rev. 1963;130:1783. doi: 10.1103/PhysRev.130.1783
[48] Chen K, Ferrenberg AM, Landau D. Static critical behavior of three-dimensional classical Heisenberg models: a high-resolution Monte Carlo study. Phys Rev B. 1993;48:3249. doi: 10.1103/PhysRevB.48.3249
[49] Fidler J, Schrefl T. Micromagnetic modelling - the current state of the art. J Phys D Appl Phys. 2000;33:R135. doi: 10.1088/0022-3727/33/15/201
[50] Srivastava CM, Aiyar R. Spin wave stiffness constants in some ferrimagnetics. J Phys C Solid St Phys. 1987;20:1119. doi: 10.1088/0022-3719/20/8/013
[51] Brockhouse BN, Watanabe H. Spin Waves in Magnetite from Neutron Scattering. Proceedings of the symposium on inelastic scattering of neutrons in solids and liquids, vol II. Vienna, Austria: IAEA; 1963. p. 297–308. https://inis.iaea.org/collection/NCLCollectionStore/_Public/44/053/44053909.pdf?r=1
[52] Heider F, Williams W. Note on temperature dependence of exchange constant in magnetite. Geophys Res Lett. 1988;15:184–187. doi: 10.1029/GL015i002p00184
[53] Kouvel JS. Specific heat of a magnetite crystal at liquid helium temperatures. Phys Rev. 1956;102:1489. doi: 10.1103/PhysRev.102.1489
[54] Moskowitz BM, Halgedahl SL. Theoretical temperature and grain-size dependence of domain state in x= 0.6 titanomagnetite. J Geophys Res Solid Earth. 1987;92:10667–10682. doi: 10.1029/JB092iB10p10667
[55] Dutz S, Hergt R. Magnetic nanoparticle heating and heat transfer on a microscale: basic principles, realities and physical limitations of hyperthermia for tumour therapy. Int J Hyperth. 2013;29:790–800. doi: 10.3109/02656736.2013.822993
[56] Usov NA, Gudoshnikov SA, Serebryakova ON, et al. Properties of dense assemblies of magnetic nanoparticles promising for application in biomedicine. J Supercond Nov Magn. 2013;26:1079–1083. doi: 10.1007/s10948-012-1974-6
[57] Fukushima H, Nakatani Y, Hayashi N. Volume average demagnetizing tensor of rectangular prisms. IEEE Trans Magn. 1998;34:193–198. doi: 10.1109/20.650225
[58] Morrish AH. Thermal, relaxation, and resonance phenomena in paramagnetic materials. John Wiley & Sons, Ltd; 2013. Chapter 3; p. 78–148. doi: 10.1002/9780470546581
[59] Newell AJ, Williams W, Dunlop DJ. A generalization of the demagnetizing tensor for nonuniform magnetization. J Geophys Res Solid Earth. 1993;98:9551–9555. doi: 10.1029/93JB00694
[60] Pokhrel A, Nepal B, Karki U, et al. Influence of layer dependent perpendicular anisotropy on higher-order anisotropies in thin films. J Magn Magn Mater. 2022;563:169963. doi: 10.1016/j.jmmm.2022.169963
[61] Plumer M, Rogers M, Meloche E. Impact of anisotropic exchange on mh loops: application to ecc media. IEEE Trans Magn. 2009;45:3942–3945. doi: 10.1109/TMAG.2009.2021852
[62] Gilbert TL. A phenomenological theory of damping in ferromagnetic materials. IEEE Trans Magn. 2004;40:3443–3449. doi: 10.1109/TMAG.2004.836740
[63] Arias R, Mills DL. Extrinsic contributions to the ferromagnetic resonance response of ultrathin films. Phys Rev B. 1999;60:7395. doi: 10.1103/PhysRevB.60.7395

[64] Azevedo A, Oliveira AB, De Aguiar FM, et al. Extrinsic contributions to spin-wave damping and renormalization in thin Ni 50 Fe 50 films. Phys Rev B. 2000 Sep;62:5331–5333. doi: 10.1103/PhysRevB.62.5331
[65] Lindner J, Barsukov I, Raeder C, et al. Two-magnon damping in thin films in case of canted magnetization: theory versus experiment. Phys Rev B. 2009 Dec;80:224421. doi: 10.1103/PhysRevB.80.224421
[66] Song HS, Lee KD, You CY, et al. Intrinsic and extrinsic Gilbert damping in exchange-biased IrMn/Cu/CoFe trilayer films. Appl Phys Express. 2015 May;8:053002. Available from: https://iopscience.iop.org/article/10.7567/APEX.8.053002
[67] Wu S, Smith DA, Nakarmi P, et al. Room-temperature intrinsic and extrinsic damping in polycrystalline Fe thin films. Phys Rev B. 2022 May;105:174408. doi: 10.1103/PhysRevB.105.174408
[68] Brown WF Jr. Thermal fluctuations of a single-domain particle. Phys Rev. 1963;130:1677. doi: 10.1103/PhysRev.130.1677
[69] Bertotti G, Mayergoyz ID, Serpico C. Nonlinear magnetization dynamics in nanosystems. Amsterdam: Elsevier; 2009.
[70] Zhao Z, Garraud N, Arnold DP, et al. Effects of particle diameter and magnetocrystalline anisotropy on magnetic relaxation and magnetic particle imaging performance of magnetic nanoparticles. Phys Med Biol. 2020;65:025014. doi: 10.1088/1361-6560/ab5b83
[71] Leliaert J, Mulkers J, De Clercq J, et al. Adaptively time stepping the stochastic landau-Lifshitz-gilbert equation at nonzero temperature: implementation and validation in mumax3. AIP Adv. 2017;7. doi: 10.1063/1.5003957
[72] Donahue MJ, Porter DG. Oommf user's guide, version 1.0, interagency report nistir 6376. Gaithersburg (MD): National Institute of Standards and Technology; 1999. Available from: https://math.nist.gov/oommf/
[73] Leliaert J, Vansteenkiste A, Coene A, et al. Vinamax: a macrospin simulation tool for magnetic nanoparticles. Med Biol Eng Comput. 2015;53:309–317. Available from: https://jleliaert.github.io/vinamax/
[74] Vansteenkiste A, Van de Wiele B. Mumax: a new high-performance micromagnetic simulation tool. J Magn Magn Mater. 2011;323:2585–2591. doi: 10.1016/j.jmmm.2011.05.037
[75] Leliaert J, Dvornik M, Mulkers J, et al. Fast micromagnetic simulations on gpu - recent advances made with mumax3. J Phys D Appl Phys. 2018;51:123002. Available from: https://mumax.github.io
[76] Scholz W, Fidler J, Schrefl T, et al. Scalable parallel micromagnetic solvers for magnetic nanostructures. Comput Mater Sci. 2003;28:366–383. Available from: http://www.magpar.net/
[77] Fischbacher T, Franchin M, Bordignon G, et al. A systematic approach to multiphysics extensions of finite-element-based micromagnetic simulations: Nmag. IEEE Trans Magn. 2007;43:2896–2898. Available from: https://nmag-project.github.io/
[78] Szambolics H, Buda-Prejbeanu LD, Toussaint JC, et al. Finite element formalism for micromagnetism. COMPEL Int J Comput Math Electr Electron Eng. 2008;27:266–276. Available from: https://feellgood.neel.cnrs.fr/
[79] Abert C, Exl L, Bruckner F, et al. Magnum.Fe: a micromagnetic finite-element simulation code based on FEniCS. J Magn Magn Mater. 2013;345:29–35. Available from: http://micromagnetics.org/magnum.fe/
[80] Leliaert J, Mulkers J. Tomorrow's micromagnetic simulations. J Appl Phys. 2019 May;125:180901. doi: 10.1063/1.5093730

[81] Garanin D, Chubykalo-Fesenko O. Thermal fluctuations and longitudinal relaxation of single-domain magnetic particles at elevated temperatures. Phys Rev B. 2004;70:212409. doi: 10.1103/PhysRevB.70.212409
[82] Kazantseva N, Hinzke D, Nowak U, et al. Towards multiscale modeling of magnetic materials: simulations of fept. Phys Rev B. 2008;77:184428. doi: 10.1103/PhysRevB.77.184428
[83] Dobrovitski V, Katsnelson M, Harmon B. Statistical coarse-graining as an approach to multiscale problems in magnetism. J Magn Magn Mater. 2000;221:L235–L242. doi: 10.1016/S0304-8853(00)00492-3
[84] Dobrovitski VV, Katsnelson MI, Harmon BN. Length scale coupling for nonlinear dynamical problems in magnetism. Phys Rev Lett. 2003 Feb;90:067201. doi: 10.1103/PhysRevLett.90.067201
[85] Feng X, Visscher PB. Coarse-graining Landau–Lifshitz damping. J Appl Phys. 2001;89:6988–6990. doi: 10.1063/1.1355328
[86] Grinstein G, Koch RH. Coarse graining in micromagnetics. Phys Rev Lett. 2003;90:207201. doi: 10.1103/PhysRevLett.90.207201
[87] Kirschner M, Schrefl T, Dorfbauer F, et al. Cell size corrections for nonzero-temperature micromagnetics. J Appl Phys. 2005;97:10E301. doi: 10.1063/1.1846411
[88] Kirschner M, Schrefl T, Hrkac G, et al. Relaxation times and cell size in nonzero-temperature micromagnetics. Physica B Condens Matter. 2006;372:277–281. doi: 10.1016/j.physb.2005.10.066
[89] Jourdan T, Marty A, Lançon F. Multiscale method for Heisenberg spin simulations. Phys Rev B. 2008 Jun;77:224428. doi: 10.1103/PhysRevB.77.224428
[90] Oezelt H, Qu L, Kovacs A, et al. Full-spin-wave-scaled stochastic micromagnetism for mesh-independent simulations of ferromagnetic resonance and reversal. Npj Comput Mater. 2022;8:35. doi: 10.1038/s41524-022-00719-5
[91] Ellis M, Evans R, Ostler T, et al. The landau-Lifshitz equation in atomistic models. Low Temp Phys. 2015;41:705–712. doi: 10.1063/1.4930971
[92] Ma PW, Dudarev S, Woo C. SPILADY: a parallel CPU and GPU code for spin–lattice magnetic molecular dynamics simulations. Comput Phys Commun. 2016;207:350–361. Available from: https://ccfe.ukaea.uk/resources/spilady/
[93] Tranchida J, Plimpton S, Thibaudeau P, et al. Massively parallel symplectic algorithm for coupled magnetic spin dynamics and molecular dynamics. J Comput Phys. 2018;372:406–425. doi: 10.1016/j.jcp.2018.06.042
[94] Cooke IJ, Lukes J. An implicit spin lattice dynamics integrator in LAMMPS. Comput Phys Commun. 2022;271:271. doi: 10.1016/j.cpc.2021.108203
[95] Omelyan I, Mryglod I, Folk R. Algorithm for molecular dynamics simulations of spin liquids. Phys Rev Lett. 2001;86:898. doi: 10.1103/PhysRevLett.86.898
[96] Perera D, Vogel T, Landau D. Magnetic phase transition in coupled spin-lattice systems: a replica-exchange Wang-Landau study. Phys Rev E. 2016;94. doi: 10.1103/PhysRevE.94.043308
[97] Ma PW, Dudarev S, Wróbel J. Dynamic simulation of structural phase transitions in magnetic iron. Phys Rev B. 2017;96. doi: 10.1103/PhysRevB.96.094418
[98] Perera D, Eisenbach M, Nicholson D, et al. Reinventing atomistic magnetic simulations with spin-orbit coupling. Phys Rev B. 2016;93. doi: 10.1103/PhysRevB.93.060402
[99] Nieves P, Tranchida J, Arapan S, et al. Spin-lattice model for cubic crystals. Phys Rev B. 2021;103. doi: 10.1103/PhysRevB.103.094437
[100] Strungaru M, Ellis M, Ruta S, et al. Spin-lattice dynamics model with angular momentum transfer for canonical and microcanonical ensembles. Phys Rev B. 2021;103. doi: 10.1103/PhysRevB.103.024429

[101] Déjardin JL, Vernay F, Kachkachi H. Specific absorption rate of magnetic nanoparticles: nonlinear AC susceptibility. J Appl Phys. 2020;128:143901. doi: 10.1063/5.0018685
[102] Dos Santos G, Aparicio R, Linares D, et al. Size- and temperature-dependent magnetization of iron nanoclusters. Phys Rev B. 2020;102. doi: 10.1103/PhysRevB.102.184426
[103] Pankhurst QA, Connolly J, Jones SK, et al. Applications of magnetic nanoparticles in biomedicine. J Phys D Appl Phys. 2003;36:R167–R181. doi: 10.1088/0022-3727/36/13/201
[104] McNamara K, Tofail SAM. Nanoparticles in biomedical applications. Adv Phys X. 2017 Jan;2:54–88. doi: 10.1080/23746149.2016.1254570
[105] Usov N, Rytov R, Bautin V. Properties of assembly of superparamagnetic nanoparticles in viscous liquid. Sci Rep. 2021;11. doi: 10.1038/s41598-021-86323-x
[106] Gubanova E, Rytov R, Usov N. Dynamics of particles with cubic magnetic anisotropy in a viscous liquid. J Magn Magn Mater. 2022;541:541. doi: 10.1016/j.jmmm.2021.168494
[107] Enpuku K, Elrefai A, Gotou J, et al. Difference in ac magnetization between suspended and immobilized magnetic nanoparticles in Néel-relaxation dominant case: effect of easy axis alignment in suspended nanoparticles. J Appl Phys. 2021;130. doi: 10.1063/5.0056481
[108] Elrefai A, Enpuku K, Yoshida T. Effect of easy axis alignment on dynamic magnetization of immobilized and suspended magnetic nanoparticles. J Appl Phys. 2021;129. doi: 10.1063/5.0041215
[109] Lyutyy T, Hryshko O, Yakovenko M. Uniform and nonuniform precession of a nanoparticle with finite anisotropy in a liquid: opportunities and limitations for magnetic fluid hyperthermia. J Magn Magn Mater. 2019;473:198–204. doi: 10.1016/j.jmmm.2018.10.074
[110] Lyutyy T, Hryshko O, Kovner A, et al. Precession of a fine magnetic particle with finite anisotropy in a viscous fluid. J Nano Electron Phys. 2016;8:04086–1–04086–5. doi: 10.21272/jnep.8(4(2)).04086
[111] Lyutyy T, Hryshko O, Kovner A. Power loss for a periodically driven ferromagnetic nanoparticle in a viscous fluid: the finite anisotropy aspects. J Magn Magn Mater. 2018;446:87–94. doi: 10.1016/j.jmmm.2017.09.021
[112] Usadel KD, Storozhenko A, Arefyev I, et al. Frequency-dependent conversion of the torque of a rotating magnetic field on a ferrofluid confined in a spherical cavity. Soft Matter. 2019;15:9018–9030. doi: 10.1039/C9SM01311C
[113] Zhao Z, Rinaldi C. Magnetization dynamics and energy dissipation of interacting magnetic nanoparticles in alternating magnetic fields with and without a static bias field. J Phys Chem C. 2018;122:21018–21030. doi: 10.1021/acs.jpcc.8b04071
[114] Trisnanto S, Ota S, Takemura Y. Two-step relaxation process of colloidal magnetic nanoclusters under pulsed fields. Appl Phys Express. 2018;11:075001. doi: 10.7567/APEX.11.075001
[115] Mamiya H, Jeyadevan B. Hyperthermic effects of dissipative structures of magnetic nanoparticles in large alternating magnetic fields. Sci Rep. 2011;1:157. doi: 10.1038/srep00157
[116] Usov NA, Liubimov BY. Dynamics of magnetic nanoparticle in a viscous liquid: application to magnetic nanoparticle hyperthermia. J Appl Phys. 2012;112:023901. doi: 10.1063/1.4737126
[117] Usadel KD. Dynamics of magnetic nanoparticles in a viscous fluid driven by rotating magnetic fields. Phys Rev B. 2017;95:104430. doi: 10.1103/PhysRevB.95.104430
[118] Engelmann UM, Shasha C, Teeman E, et al. Predicting size-dependent heating efficiency of magnetic nanoparticles from experiment and stochastic Néel-Brown Langevin simulation. J Magn Magn Mater. 2019;471:450–456. doi: 10.1016/j.jmmm.2018.09.041

[119] Usadel KD. Private communication. 2020.
[120] Maralescu FM, Bende F, Sporea I, et al. Non-invasive evaluation of kidney elasticity and viscosity in a healthy cohort. Biomedicines. 2022;10:2859. doi: 10.3390/biomedicines10112859
[121] García-Palacios JL, Lázaro FJ. Langevin-dynamics study of the dynamical properties of small magnetic particles. Phys Rev B. 1998;58:14937–14958. doi: 10.1103/PhysRevB.58.14937
[122] Usadel KD. Temperature-dependent dynamical behavior of nanoparticles as probed by ferromagnetic resonance using Landau-Lifshitz-gilbert dynamics in a classical spin model. Phys Rev B. 2006;73:212405. doi: 10.1103/PhysRevB.73.212405
[123] Allen M, Tildesley D. Computer simulation of liquids. Oxford: Oxford University Press; 1989.
[124] Fazeli A, Thakore V, Ala-Nissila T, et al. Non-Stokesian dynamics of magnetic helical nanoswimmers under confinement. PNAS Nexus. 2024;3:182. doi: 10.1093/pnasnexus/pgae182